

The dynamics of the hydrogen exchange reaction at 2.20 eV collision energy: Comparison of experimental and theoretical differential cross sections

E. Wrede,^{a)} L. Schnieder,^{b)} and K. H. Welge

Fakultät für Physik, Universität Bielefeld, Postfach 100131, 33501 Bielefeld, Germany

F. J. Aoiz, L. Bañares, J. F. Castillo, and B. Martínez-Haya

Departamento de Química Física, Facultad de Química. Universidad Complutense. 28040 Madrid, Spain

V. J. Herrero

Instituto de Estructura de la Materia (CSIC). Serrano 123. 28006 Madrid, Spain

(Received 28 December 1998; accepted 3 March 1999)

The $\text{H} + \text{D}_2(v=0, j=0) \rightarrow \text{HD}(v', j') + \text{D}$ isotopic variant of the hydrogen atom exchange reaction has been studied in a crossed molecular beam experiment at a collision energy of 2.20 eV. Kinetic energy spectra of the nascent D atoms were obtained by using the Rydberg atom time-of-flight technique. The extensive set of spectra collected has permitted the derivation of rovibrationally state-resolved differential cross sections in the center-of-mass frame for most of the internal states of the HD product molecules, allowing a direct comparison with theoretical predictions. Accurate 3D quantum mechanical calculations have been carried out on the refined version of the latest Boothroyd–Keogh–Martin–Peterson potential energy surface, yielding an excellent agreement with the experimentally determined differential cross sections. The comparison of the results from quasi-classical trajectory calculations on the same potential surface reveals some discrepancies with the measured data, but shows a good global accordance. The theoretical calculations demonstrate that, at this energy, reactive encounters are predominantly noncollinear and that collinear collisions lead mostly to nonreactive recrossing. The experimental results are satisfactorily accounted for by theoretical calculations without consideration of Geometric Phase effects. © 1999 American Institute of Physics. [S0021-9606(99)01420-8]

I. INTRODUCTION

In a series of recent works,^{1–6} rovibrationally state-resolved differential cross sections (DCS) have been experimentally determined for the $\text{H} + \text{D}_2(v=0, j=0) \rightarrow \text{HD}(v', j') + \text{D}$ reaction over a wide range of collision energies. The DCSs were derived from kinetic energy spectra (KES) of the nascent D atoms measured with the Rydberg atom time-of-flight (TOF) technique developed at the University of Bielefeld.⁷ The experimental data available at present correspond to collision energies (E_{col}) of 0.52–0.54 eV, 1.27–1.30 eV, 2.20 eV and 2.67 eV, and the simulation of the measurements with theoretical calculations has provided a most valuable information about the dynamics of the prototypic hydrogen atom exchange reaction.

For the collision energies experimentally accessed until now, the reactivity of this system should be largely determined by the lowest adiabatic potential hypersurface. There are various *ab initio* versions of the lowest potential energy surface (PES), termed LSTH,^{8,9} DMBE,¹⁰ BKMP,¹¹ and BKMP2.¹² The differences between these PESs are small, and dynamical calculations performed on them lead mostly to very similar results, usually indiscernible by comparison

with experiment. Only in a few occasions have the theoretical predictions suggested that such subtle differences in the shape of the PESs could have a noticeable influence on the observations. This happened, for instance, in the theoretical studies of low temperature rate constants.^{13–17} In particular, the quantum mechanical reaction rate coefficients calculated by Mielke *et al.*¹³ for the $\text{D} + \text{H}_2$ reaction on the LSTH and DMBE PESs, were in surprisingly better agreement with the measurements than those on the more recent BKMP¹³ and BKMP2¹⁷ PESs, based on a larger set of *ab initio* points. However, a detailed comparison of accurate quantum mechanical (QM) calculations with the Rydberg TOF spectra at $E_{\text{col}} = 0.52\text{--}0.54$ eV (Ref. 6) has allowed a direct assessment of the quality of the different surfaces and favors strongly the newest BKMP2 PES. In a similar way, the determination of state-resolved DCS in the 1.27–1.30 eV collision energy range³ excluded the presence of a scattering resonance obtained in QM calculations on the LSTH PES by Kuppermann and Wu¹⁸ when geometrical phase (GP) effects were included.

A particularly thorough investigation was conducted at $E_{\text{col}} = 0.53$ eV and 1.28 eV.^{1,2} The extensive set of KES collected in the laboratory (LAB) frame allowed for the determination of rovibrationally state-resolved DCSs in the center-of-mass (CM) system,² thus making possible the direct comparison of the measurements with the predictions of theoretical calculations. The experimental data at the higher

^{a)}Corresponding author. Present address: School of Chemistry, University of Bristol, Cantock's Close, Bristol BS8 1TS, U.K. Email: eckart.wrede@bristol.ac.uk

^{b)}Present address: Zentrum für Medizinische Forschung, Waldhörnlestr. 22, D-72072 Tübingen, Germany.

collision energy, $E_{\text{col}} = 1.28$ eV, are very well accounted for by the results of accurate QM calculations, and only slightly worse by those from quasiclassical trajectories (QCT).¹ For the lower collision energy, $E_{\text{col}} = 0.53$ eV, the QCT calculations give still a good estimate of the integral cross section, but fail to reproduce the shape of the rotationally state resolved DCS.²

The experiments carried out at higher collision energies explore a region characterized worse from a theoretical viewpoint, since most of the *ab initio* effort^{8,10–12} has been invested in the neighborhood of the classical barrier to reaction and, furthermore, no accurate QM scattering calculations of the reaction dynamics have been published for collision energies above 2 eV. With increasing energy, the first electronically excited state may start affecting the reaction dynamics. In fact, theoretical studies by Kuppermann and Wu suggest^{19–21} that GP effects associated with the conical intersection between the two lowest potential surfaces might have a direct influence on dynamical observables, even for energies clearly below that of the conical intersection. Although the predictions indicate that GP effects should be more pronounced for DCSs than for integral cross sections,²² they could not be identified until now in any of the measured state-resolved DCSs, and the experimental evidence in favor of GP effects comes from lower resolution measurements of integral cross sections.^{23,24} In addition, for energies higher than that of the conical intersection, nonadiabatic transitions could also play a role in the reactivity.

State-resolved scattering measurements carried out at a collision energy of 2.67 eV (corresponding to a total energy of 2.86 eV, thus above that of the minimum energy of the conical intersection) could be well simulated with the results of QCT calculations on the BKMP2 PES,⁵ indicating that, even at this high energy, the influence of the upper electronic state is small and that the essentials of the dynamics are describable by a classical motion of the nuclei on the lowest adiabatic PES.

In a recent letter,⁴ the first results of a Rydberg atom TOF experiment at a collision energy of 2.2 eV were presented. Experimental KES were reported at various LAB scattering angles, and these measurements were simulated with QCT calculations performed on the LSTH and DMBE PESs, yielding a global good agreement with the experimental data. This collision energy is of interest because experimental results from other techniques are available for comparison.^{25,26}

In the present article, we describe the results of a detailed experimental study of the reaction dynamics at $E_{\text{col}} = 2.2$ eV. Rovibrationally state-resolved DCSs have been obtained in the CM frame for most internal states of the nascent HD molecules. In addition, accurate QM calculations have been performed at this energy on the BKMP2 PES, using the methodology developed by Manolopoulos and Castillo.²⁷ The experimental measurements have been simulated with the QM DCS, as well as with those obtained by QCT calculations performed on the same PES. The dynamical behavior of the reaction at this collision energy is discussed, and the results from the two theoretical approaches are compared.

II. EXPERIMENTAL AND THEORETICAL METHODS

A. Experiment

The experimental setup has been described in detail in Refs. 2 and 28, and only a brief account is given here. A pulsed molecular beam of *ortho*-D₂, adiabatically cooled to the ground rotational state ($j=0$) in a supersonic expansion from a liquid N₂ cooled reservoir, was crossed at right angles with kinematically hot H atoms, generated by the photolysis of HI in a second molecular beam (parallel to the D₂ one at a distance of 30 mm) with linearly polarized 212.81 nm light (fifth harmonic of the Nd:YAG laser). The direction of polarization of the photolysis light was chosen to direct the *fast* H atoms, corresponding to the formation of I(²P_{3/2}), toward the scattering center in the D₂ beam. The most probable velocities of the H atoms and D₂ molecules were 22.945 ± 10 m/s and 1045 ± 38 m/s, respectively, resulting in an average collision energy of $E_{\text{col}} = 2.204 \pm 0.006$ eV, with the errors giving the spreads (full-width-half-maxima, FWHM) of the corresponding distributions. The velocity distribution of the nascent D atoms was measured using the technique of Rydberg atom time-of-flight (TOF) spectroscopy,⁷ which is based on the resonant excitation of the D atoms into metastable Rydberg states directly inside the scattering volume with nanosecond pulsed laser radiation of 121.6 nm and 366 nm wavelengths. The excited atoms depart from the scattering region due to their laboratory (LAB) velocity, and are detected at the end of the drift region by field ionization and subsequent acceleration of the ions onto a particle multiplier. The detector can be rotated around the scattering center in the plane defined by the central axes of the particle beams and has an angle of acceptance of 1° in this plane and 5° perpendicular to it. With a drift path length of 305 mm, the energy resolution ($\Delta E/E$) of the TOF measurement itself is $\approx 0.5\%$.

D atom TOF spectra were recorded at 20 LAB scattering angles between -5° and 70° ; the LAB angular origin being chosen in the direction of the H atom beam. Accumulation times of 1–2 h (i.e., from 36 000 to 72 000 laser pulses at 10 Hz repetition rate) were necessary to collect about 50 000 D atoms and to get reasonable statistics as can be seen in the spectra shown below. The LAB angular distribution (AD) of the total scattered signal was obtained by integrating the D atom signal at every angle for 300 s with typical count rates up to 9 s^{-1} . The velocity and angular spreads of the molecular beams, together with the detector angle of acceptance and the resolution of the TOF measurement, limit the experimental resolution of the LAB kinetic energy and the CM scattering angle. Both of them also depend on the LAB scattering angle and the D atom speed.²⁸ At LAB angles close to 0° , the kinetic energy resolution ranged from 15 meV for slow D atoms (HD molecules with high internal energy) to 17 meV for fast D atoms (HD with low internal energy). At $\Theta_{\text{Lab}} = 70^\circ$, the corresponding range was 30–66 meV, respectively.

B. Theory

All the theoretical calculations have been carried out on the BKMP2 PES.¹² The QM reactive scattering calculations

have been performed for the $\text{H}+\text{D}_2(v=0, j=0)$ reaction using a coupled-channel hyperspherical coordinate method²⁷ at a total energy of 2.3917 eV, which corresponds to the collision energy of the experiment ($E_{\text{col}}=2.20$ eV). In order to obtain integral and differential cross sections, the calculations have been performed for a large number of total angular momenta J . The convergence parameters are E_{max} , j_{max} , and K_{max} . The first two parameters define the coupled-channel basis set, which contains all $\text{H}+\text{D}_2$ and $\text{HD}+\text{D}$ channels with diatomic energy levels $E \leq E_{\text{max}}$ and rotational quantum numbers $j \leq j_{\text{max}}$. Convergence tests for vibrationally state-resolved reaction probabilities for the $\text{H}+\text{D}_2(v=0, j=0)$ reaction have been performed at $J=0$ as a function of E_{max} and j_{max} at the collision energy of 2.20 eV. It has been found that reaction probabilities are converged to better than 1% by using $E_{\text{max}}=2.85$ eV and $j_{\text{max}}=20$. The convergence parameter K_{max} is only relevant for $J>0$, where it serves as an upper limit on the helicity quantum number K . The convergence with respect to K_{max} was checked at the total angular momentum $J=16$. It was found that at this J value the reaction probabilities were all well converged by retaining angular basis functions with all allowed helicity quantum numbers up to $K_{\text{max}}=12$ in both the reactant and product arrangements. Therefore, the production parameters for the present calculations are $E_{\text{max}}=2.85$ eV, $j_{\text{max}}=20$, and $K_{\text{max}}=12$. The use of these parameters results in a coupled-channel basis set containing a total of 198 channels for $J=0$, whereas for $J \geq 12$ there is a maximum number of 1672 channels. Calculations up to $J=41$ were needed to get well converged DCSs.

The details of the QCT method used for the calculations can be found in Refs. 4,29–31 and in the references cited therein. For the present study, a batch of 10^6 trajectories has been calculated on the BKMP2 PES at the collision energy of the experiments and for the ground rotational state of the D_2 molecule. The maximum impact parameter used was 1.3 Å.

The assignment of the final product quantum states is made by equating the square of the classical rotational angular momentum modulus to $j'(j'+1)\hbar^2$. With this noninteger j' “quantum” number so obtained, the vibrational quantum number v' is found by equating the internal energy of the outgoing molecule to a rovibrational Dunham expansion in $(v'+1/2)$ and $j'(j'+1)$, whose coefficients are calculated by fitting the semi-classical rovibrational energies calculated using the asymptotic diatomic limits of the BKMP2 PES. The noninteger v' and j' values are then rounded to the nearest integer. The rovibrationally state-resolved DCS were calculated by the method of moments expansion in Legendre polynomials.³⁰

The QM and QCT calculations have been carried out on the lowest adiabatic electronic surface, and no attempt has been made to incorporate into the dynamics any possible influence of the upper electronic surface like phase effects associated with the conical intersection.

The simulation of the LAB kinetic energy spectra of the scattered D atoms is performed by transforming the theoretical CM state-resolved DCSs into the LAB system using the appropriate Jacobian and geometric factors, and taking also

into account the experimental broadening. The inversion procedure is described in Refs. 2,6 and the full details are given in Ref. 28. Suffice it to say here that only one parameter is needed for scaling the experimental to the theoretical KES and LAB AD. This parameter is obtained by equating the experimental “total cross section” to the theoretical QM and QCT values. The “total cross section” values are obtained by summing over all final states and integrating over the scattering angles experimentally accessible.^{2,6} Note that, as is customary, we take the origin of the CM scattering angles ($\theta=0^\circ$) as that defined by the direction of the incoming H atom. Thus, HD product molecules scattered at $0^\circ/180^\circ$ correspond to *forward/backward* scattering. In the following, the CM DCSs refer to HD scattering, whereas the experiments and the theoretical simulations in the LAB frame and the polar map in the CM frame refer to D atom scattering.

III. RESULTS

Figures 1(a) and 1(b) display the comparison between experimental and theoretically simulated KES covering the LAB angular range between -5° and 70° . The agreement between the measured KES spectra and the simulations based on the QM calculations is excellent at all LAB angles, the measured and simulated spectra being barely distinguishable. The same experimental data can be also well reproduced globally with the results of the QCT calculation, but the degree of accordance is clearly worse, in particular with respect to the heights of the peaks corresponding to high j' states of $\text{HD}(v'=0,1)$ for the lower and higher LAB scattering angles sampled.

The experimental total LAB angular distribution of the scattered D atoms summed over all the internal states of the products is represented in Fig. 2 together with its theoretical simulations. As can be seen, the agreement between the experimental and the two theoretically simulated LAB ADs is quite good. Only in the range between $\approx 10^\circ$ and 25° , the simulated QM curve deviates slightly from the experimental points. In the QCT case, the theoretical curve shows a small shoulder somewhat higher than the experimental values in the 60° – 80° angular range. A similar effect can be observed in the QCT angular distributions obtained previously on the LSTH and DMBE PESs.⁴ As expected, the angular distribution at $E_{\text{col}}=2.2$ eV covers a wider range of LAB scattering angles than that at 1.30 eV, but narrower than at 2.67 eV,⁵ reflecting the fact that sideways scattering in the CM frame increases with collision energy.

From the present experimental data, CM DCSs for most rovibrational states of the products could be determined unambiguously up to $v'=4$ following the procedure described in Ref. 2, and could thus be compared directly to the results of dynamical calculations. A selection of CM DCSs are represented in Figs. 3(a)–3(d).³² In the cases where overlapping signals from different states had to be considered in the derivation of a given experimental v', j' DCS, these states have been indicated in parentheses. It should be recalled here, that a single “size” parameter has been used for the scaling of the whole set of rovibrationally state-resolved DCSs, following the procedure of Ref. 2, and that the extraction procedure is absolutely independent of the theoretical calculations. An

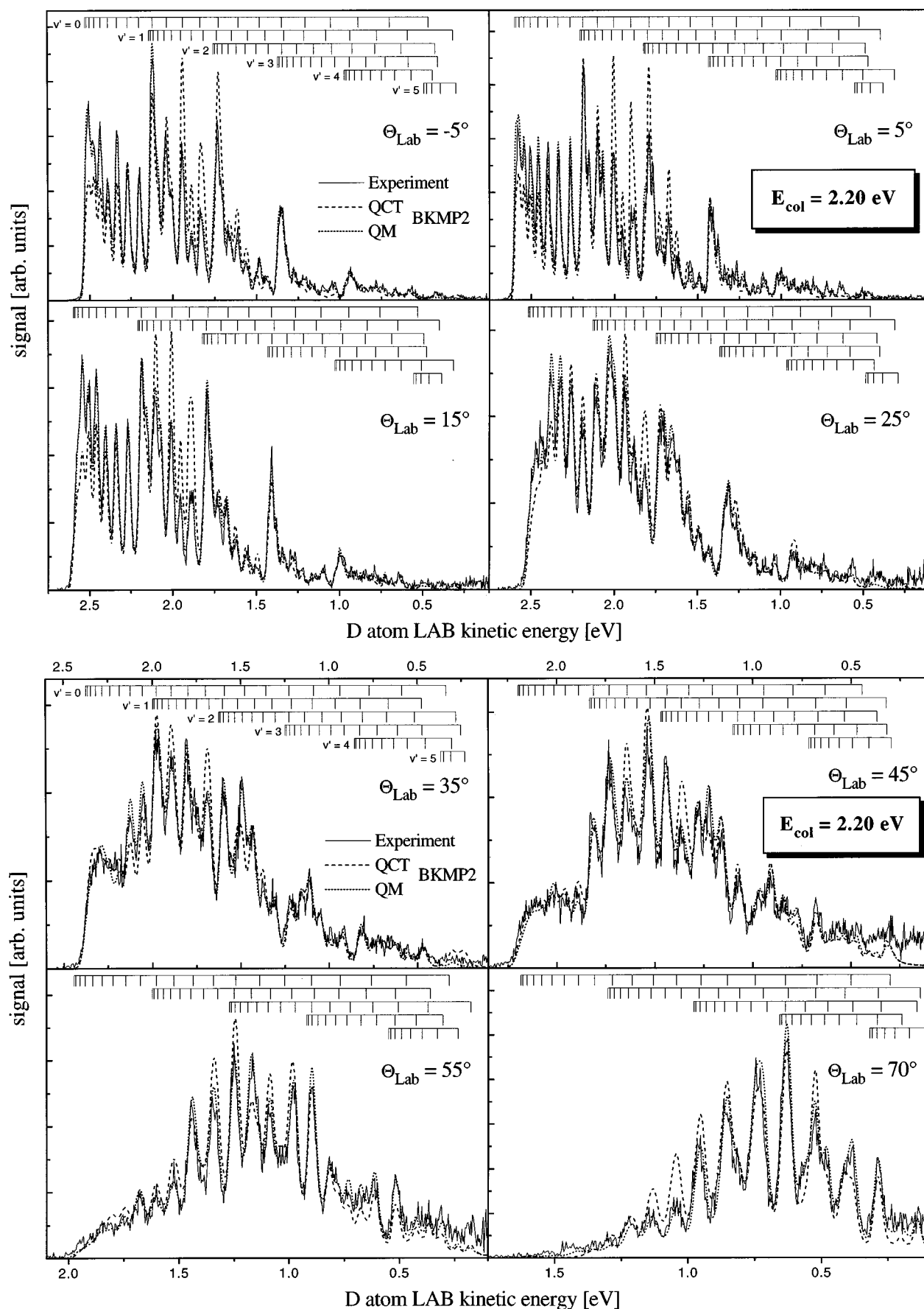


FIG. 1. LAB D atom kinetic energy spectra at the indicated LAB scattering angles Θ_{Lab} for the $\text{H} + \text{D}_2(v=0, j=0)$ reaction at the collision energy 2.20 eV. The experimental data are shown together with the simulations obtained using the QM (short-dash line) and QCT (long-dash line) v', j' DCSs calculated on the BKMP2 PES.

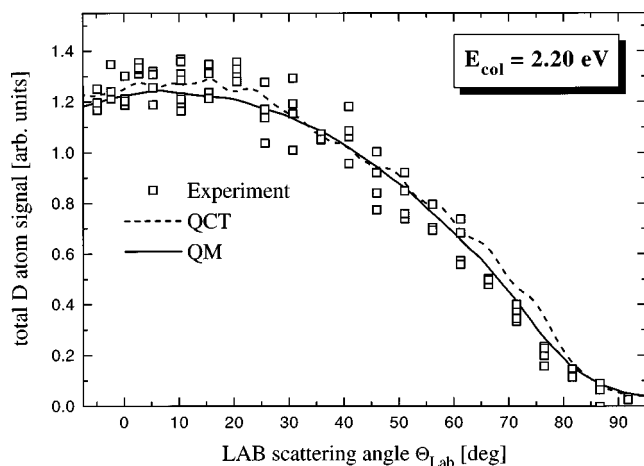


FIG. 2. D atom laboratory angular distribution for the $\text{H}+\text{D}_2(v=0, j=0)$ reaction at $E_{\text{col}}=2.2$ eV. Open squares: experimental data. Solid line: QM simulation. Dashed line: QCT simulation.

overview of the figures shows that the v', j' state-resolved DCSs at this collision energy are more structured in general than the corresponding ones at 0.53 and 1.28 eV.² As can be expected from the excellent agreement obtained in the comparison of KES, the coincidence between the experimentally derived and QM v', j' state-resolved DCSs is indeed remarkable. The few remaining discrepancies are small, and show up for those experimental DCSs where more than one HD product state contributes to the signal in the KES in the same kinetic energy range, thus preventing an unambiguous extraction. In any case, the uncertainty in the measurements and calculations is largest for the high v' states. For the $v'=0-3$ vibrational states, the angular distributions shift from backward to sideways with increasing j' . A similar tendency was observed in the experiments at ~ 1.29 eV, but not in those at ~ 0.53 eV.

A global good agreement is also obtained between experimental and QCT DCSs, but here the differences are larger. Within the individual QCT DCSs, the degree of accordance varies from a near perfect matching like the one obtained for $v'=0, j'=7, 8$, to a clear discrepancy between experimental and QCT DCSs, like those for $v'=0, j'=12, 15$, $v'=2, j'=6$ or $v'=4, j'=0$. In addition, the QCT prediction underestimates the backward scattering into the $j'=0$ state of the different vibrational levels.

The global information provided by the state-resolved DCSs can be presented as D atom CM angle-velocity polar maps as that shown in Fig. 4. The upper half corresponds to the polar map constructed by using the QM v', j' DCSs, whereas the lower half corresponds to that obtained with the experimental DCSs. Since these maps should be symmetric about the relative velocity vector, the agreement between the two sides reflects the almost perfect coincidence between QM and experimental results. As mentioned above, experimental constraints precluded measurements in the HD CM forward hemisphere and, thus, this region of the experimental map is empty.

In Fig. 5 the experimental DCS for the production of HD ($v'=4, j'=3$) are compared with the DCS measured by Xu *et al.*²⁶ by means of a photon initiated reaction technique

based on the kinematic relations using the law of cosines. The results of the QM and QCT calculation on the BKMP2 surface are also shown. The experimental data of Xu *et al.* have been scaled to the present experimental DCS. In order to compare with the present Rydberg atom TOF results having a better angular resolution, neither the QM nor the QCT DCS has been smoothed, and this should be taken into account when comparing with the experiment of Xu *et al.* which has a broad instrumental function.^{26,33} Both experimental methods are affected by large uncertainties in the relative values of the cross sections and little can be said aside from the fact that the reactive scattering is, to a great extent, isotropic. The QM DCS lies in general within the error bars of the Rydberg atom TOF data, and so does the QCT one over most of the angular range. The clearest discrepancy between experiment and QCT is found in the region around 140° ($\cos \theta_{\text{CM}} \approx -0.77$) where the two experiments, in agreement with the QM result, indicate the presence of a small local maximum, which is notably overestimated in the QCT prediction. In order to fully appreciate the comprehensiveness of the present experiment, it is worth noting that the measurements of Fig. 5 would correspond just to one of the panels displayed in Figs. 3(a)–3(d). Note also the very low absolute value of the cross section for the production of this state, and thus the very high sensitivity of the experimental techniques.

IV. DISCUSSION

In a previous work⁴ it was already noticed that the largest disagreement between experimental and QCT simulated KES spectra calculated on the LSTH and DMBE PESs was found in the peaks corresponding to the $v'=0$ and $j'=11-13$ states, which are precisely the levels with the highest population. The same conclusion can be drawn from the present results on the BKMP2 PES. Since the shapes of the QCT state-resolved DCSs do not differ in general very appreciably from the corresponding QM or experimental ones (see Fig. 3), the origin of the discrepancy must be sought in the respective value of the integral cross sections.

Figure 6 shows the comparison of QM and QCT state-resolved integral cross sections (ICS) $\sigma_{\text{R}}(v', j')$ for $v'=0-4$. The QM and QCT rotational distributions have similar shapes within each v' , but the absolute values of the cross section for the production of the individual rotational states differ notably in some cases. The largest absolute discrepancy between QM and QCT $\sigma_{\text{R}}(v', j')$ are found for the above mentioned states, $v'=0, j'=11-13$, where the QM calculations, which give very good agreement with experiment, yield clearly lower cross sections, thus justifying the failure of the QCT calculations to account for the corresponding peaks in the measured spectra.

Table I contains the vibrationally resolved ICS, summed on all final j' , obtained in the QCT and QM calculations at 2.2 eV on the BKMP2 PES. The main discrepancy corresponds to the highest accessible vibrational state, $v'=5$, where the QCT $\sigma_{\text{R}}(v')$ is almost one order of magnitude larger. This is due to the QCT binning procedure (rounding *real* v' values to the nearest integer), which allocates trajectories with less vibrational energy than that corresponding to

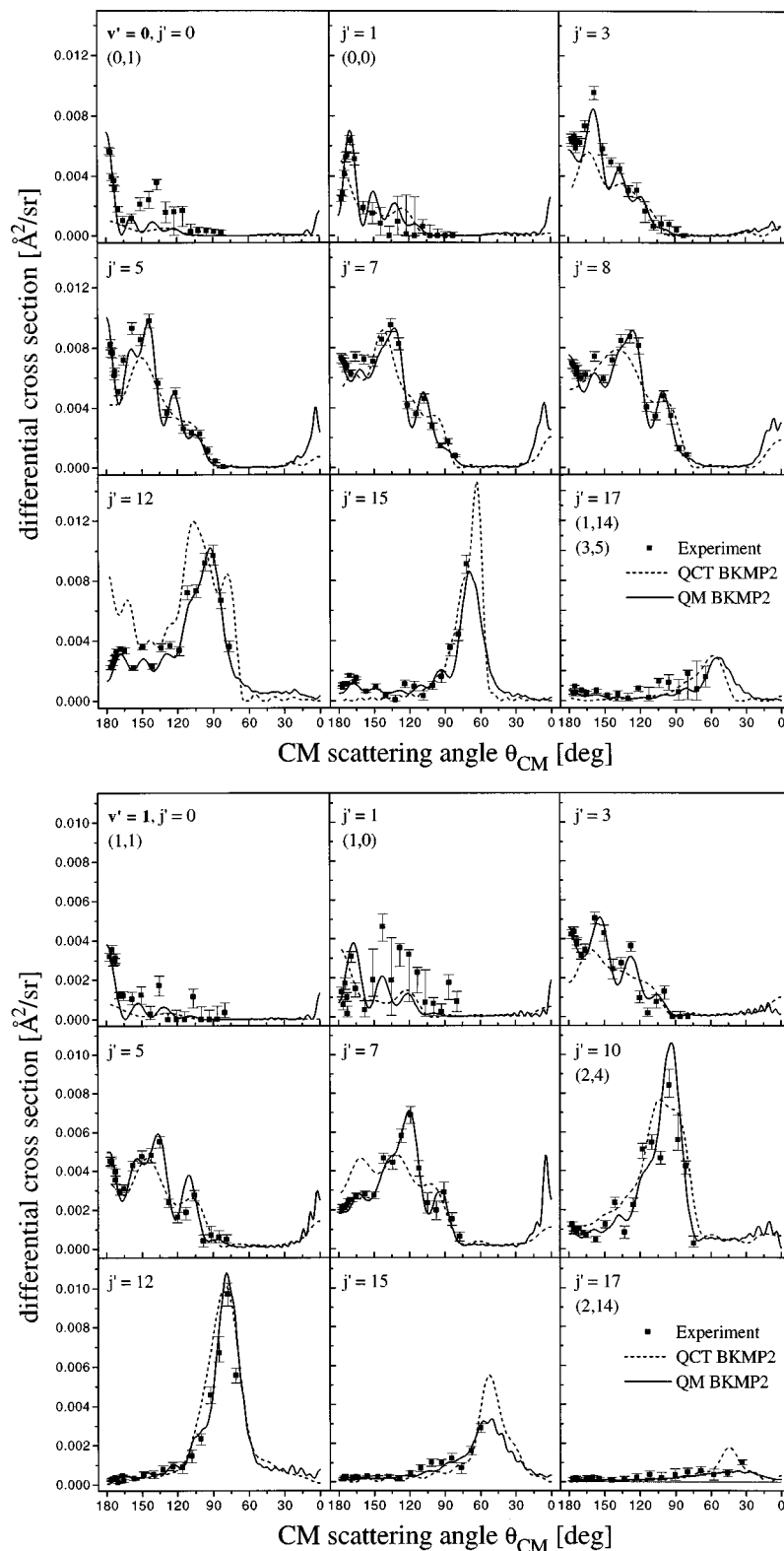


FIG. 3. Selected v', j' state-resolved DCSs in the CM system for the $\text{H} + \text{D}_2(v=0, j=0) \rightarrow \text{HD}(v', j') + \text{D}$ reaction. Solid squares with error bars: experimental results. Solid and dashed lines represent the QM and QCT results, respectively, calculated on the BKMP2 PES at collision energy of 2.20 eV. The numbers in parenthesis indicate the v', j' values of the states which overlap in the KES with the state corresponding to each panel.

this state. In addition, for $v'=0$, the QM cross section is somewhat smaller to that found in the QCT calculation, due to the overestimation of the ICSs for $j'=11-13$ discussed in the previous paragraph.

The QM and QCT total (summed over all internal states) and the vibrationally state-resolved DCSs for $v'=0-4$ are compared in Fig. 7. The general agreement between the results of both theoretical approaches is very good. Both sets

of calculations predict the appearance of forward peaks whose relative importance grows with increasing v' , but, similarly to the results obtained at 1.29 eV,³¹ the QM forward peak is larger than that obtained in the classical calculation, especially for the highest vibrational state represented. No attempt to get the total and v' state-resolved experimental DCSs has been made mainly due to the fact that the CM angular range experimentally accessible depends on the par-

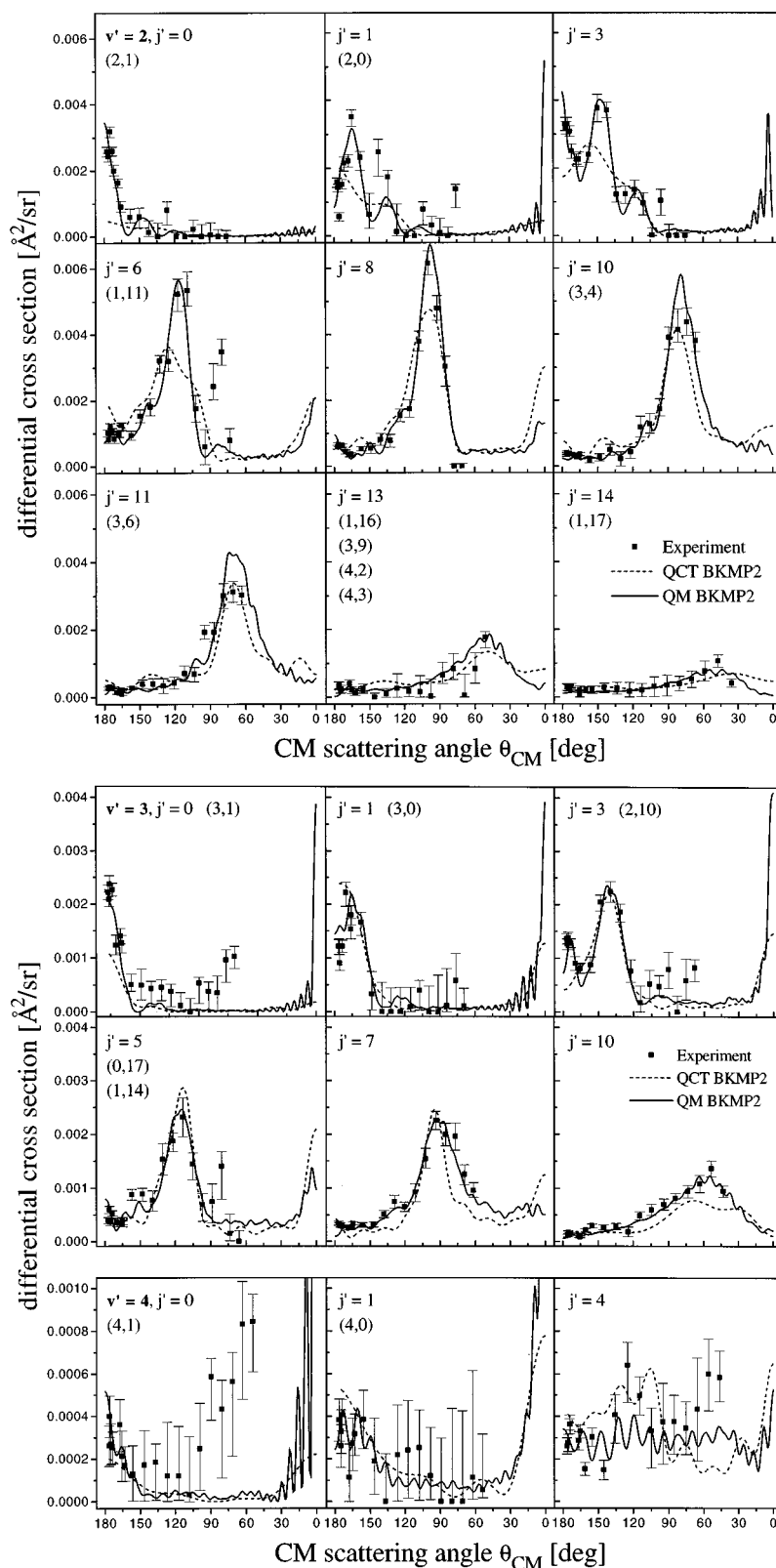


FIG. 3. (Continued.)

ticular v', j' state, as well as, to the uncertainty caused by the assignment of the signal among overlapping product states.

Figures 8(a) and 8(b) show the QM and QCT v', j' state-resolved reaction probability, $P(J)$, as a function of the total angular momentum, J . For $v' < 4$, the maxima in $P(J)$ appear at progressively larger J as the final j' increases re-

flecting a direct channeling of collisional orbital motion into rotation of the nascent HD molecules. The fact that rotationally excited HD molecules are generated predominantly in large impact parameter (high J) reactive encounters can be related to the shift from backward to sideways scattering observed in the DCSs as j' increases for a given v' , and is consistent with the intuitive expectation of correlating small

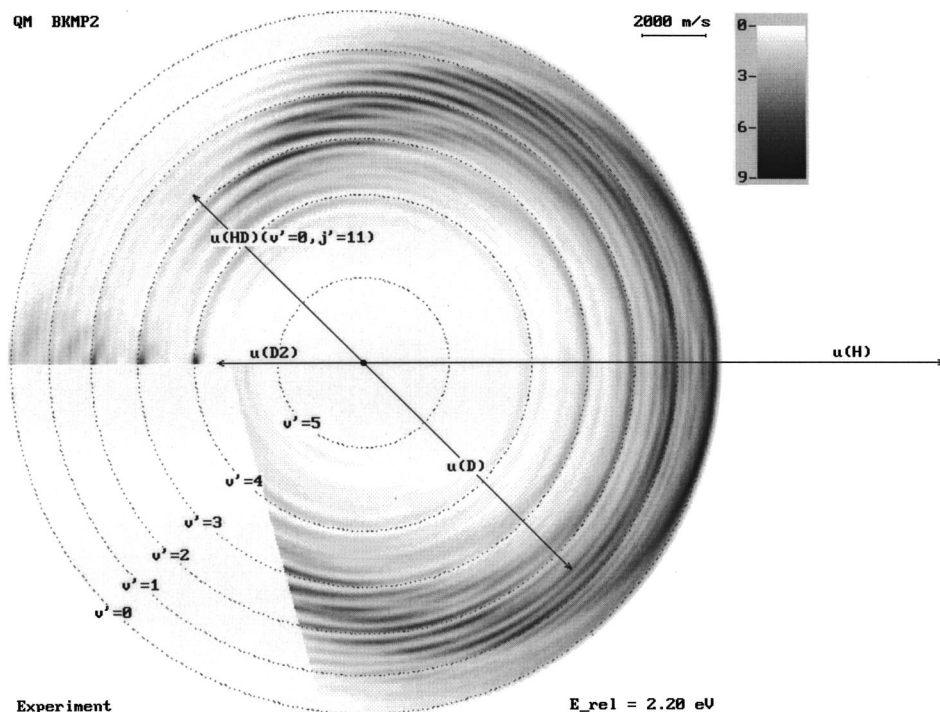


FIG. 4. Composite D atom angle-velocity polar map of the $\text{H}+\text{D}_2(v=0, j=0) \rightarrow \text{HD}+\text{D}$ reaction at 2.2 eV collision energy. The upper half has been constructed using the QM v', j' DCSs, whereas the lower half corresponds to the experimentally deduced DCSs. The arrow labeled with $u(\text{D})$ represents the D atom CM velocity vector for a given v', j' HD state. The DCS has been “smoothed” using a Gaussian profile in $u(\text{D})$ with a FWHM of 200 m/s to obtain a reasonable resolution. The intensities scale from 0 to 9 $\text{\AA}^2/(\text{sr}\cdot\text{m/s})$ as shown in the figure. The blank part of the experimental polar map represents the nonaccessible region of CM scattering angles.

impact parameters with high (backward) scattering angles and large impact parameters with low (sideways to forward) scattering angles. This behavior, common to many direct type reactions, was also found for the present system at $E_{\text{col}}=1.28 \text{ eV}$,³⁴ where, as in the present case, the $P(J)$ obtained by the two theoretical approaches were very similar. The small discrepancies found at 2.2 eV can be traced back in many cases to the ICS for production of each v', j' state, shown in Fig. 6.

For $v'=4$, however, the maxima in $P(J)$ do not shift clearly toward higher J values with increasing j' . Interestingly, this behavior for the less exoergic channels resembles that found at $E_{\text{col}}=0.53 \text{ eV}$, where the energy available is also limited, and $v'=0$ is the only populated channel.

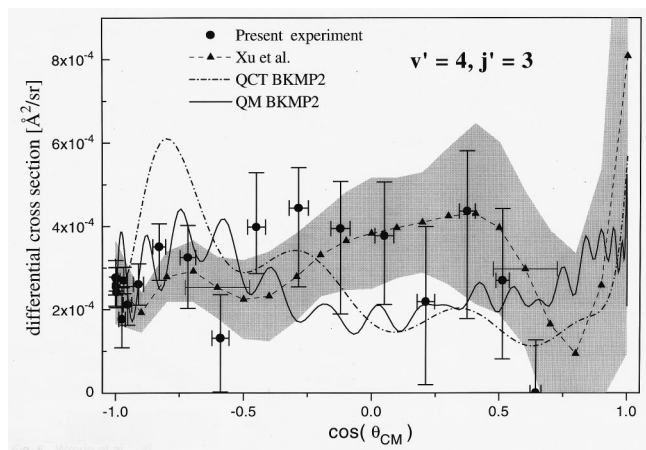


FIG. 5. State-resolved DCS in the CM system for the $\text{H}+\text{D}_2(v=0, j=0) \rightarrow \text{HD}(v'=4, j'=3)+\text{D}$ reaction. Solid circles with error bars: present experimental results. Triangles and shaded area: experimental results from Ref. 26. Solid line: QM calculation. Dot-dash line: QCT calculation.

At low energies the reaction is caused by collisions with low impact parameter yielding predominantly backward scattering. Taking into account that the lower barrier to reaction corresponds to a collinear configuration of the three nuclei, one might think at first sight that there is an inherent correlation between backward scattering and collinear encounters; however, at high collision energies this is not the case due to the nonreactive recrossing of trajectories back into the reactants valley.

The importance of classical recrossing for the collision energy investigated is addressed in Table II. This table includes the QCT reactive and nonreactive recrossing total

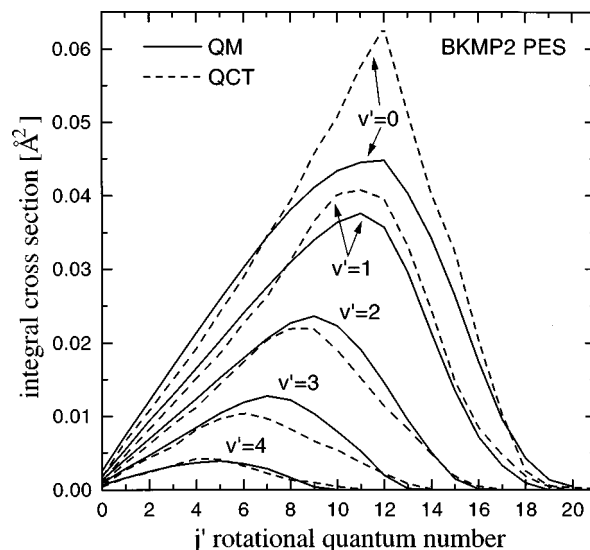


FIG. 6. QM (solid line) and QCT (dashed line) v', j' state-resolved integral cross sections for the $\text{H}+\text{D}_2(v=0, j=0)$ reaction calculated on the BKMP2 PES.

TABLE I. QM and QCT vibrationally state-resolved integral cross sections (\AA^2) for the $\text{H}+\text{D}_2(v=0, j=0) \rightarrow \text{HD}(v', j')+\text{D}$ reaction at the collision energy of 2.2 eV calculated on the BKMP2 PES. Values in parentheses are the statistical errors in the last significant figure of the QCT calculations.

v'	σ_R^{QM}	σ_R^{QCT}
0	0.497	0.555(2)
1	0.368	0.385(1)
2	0.207	0.188(1)
3	0.096	0.078(1)
4	2.4×10^{-2}	$2.5(1) \times 10^{-2}$
5	3.3×10^{-4}	$2.0(1) \times 10^{-3}$
Total	1.192	1.233(2)

cross sections at $E_{\text{col}}=1.83$ eV and $v=1, j=0$, which has the same total energy as in the present case, and at $E_{\text{col}}=2.67$ eV and $v=0, j=0$, which is the highest total energy experimentally accessed so far for the H_3 system. As can be seen, the recrossing cross sections are a significant fraction of the reaction cross sections, and its relative importance grows rapidly with collision energy but not with reagent vibration. In fact, the decrease in the reaction cross section from 2.2 to 2.67 eV is caused by the increase of recrossing collisions. In Fig. 9, reactive and recrossing trajectories for $\text{H}+\text{D}_2(v=0, j=0)$ are represented versus the bending angle at the “first crossing.” This first crossing is reached when the distance between the attacking atom and one of the other nuclei is shorter than the separation between the nuclei of the reacting molecule. Note that a bending angle of 180° implies a collinear arrangement when the system first crosses the

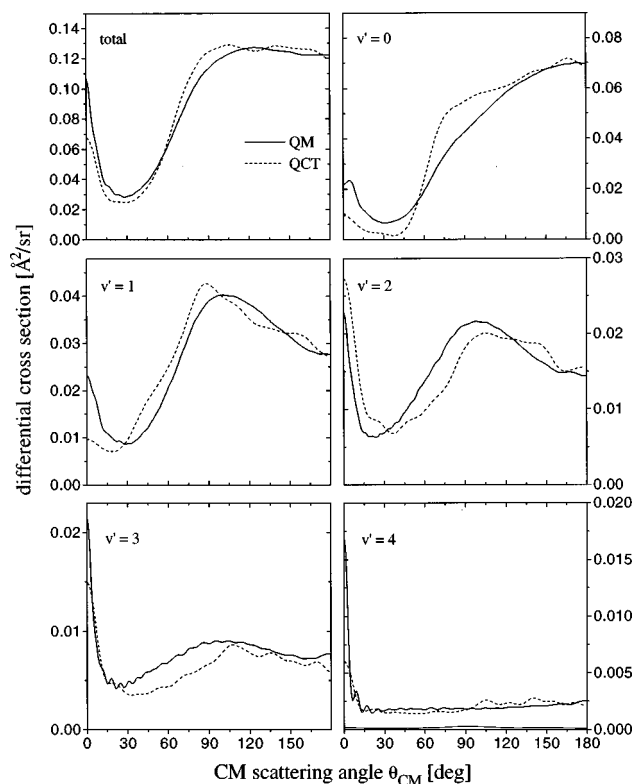


FIG. 7. Vibrationally state-resolved DCSs in the CM system for the $\text{H}+\text{D}_2(v=0, j=0) \rightarrow \text{HD}(v', j')+\text{D}$ reaction. Solid line: QM calculations. Dash line: QCT calculations.

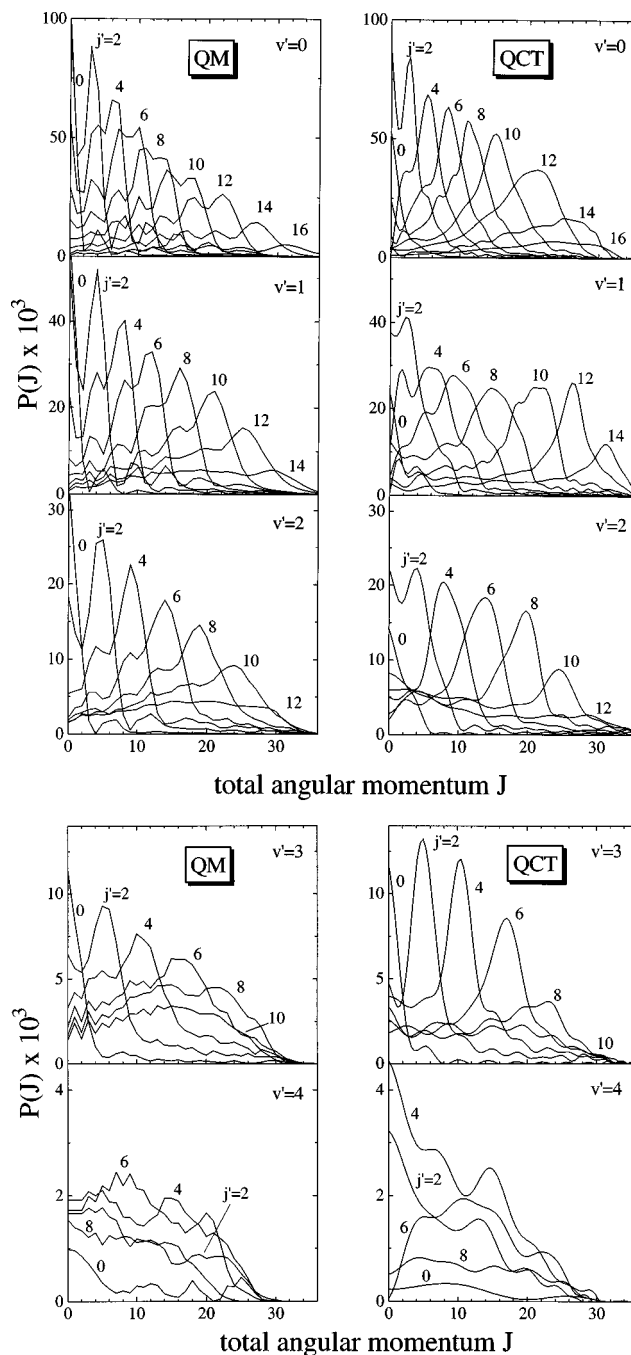


FIG. 8. QM (left) and QCT (right) reaction probability as a function of total angular momentum, J , for the $\text{H}+\text{D}_2(v=0, j=0) \rightarrow \text{HD}(v', j')+\text{D}$ reaction calculated on the BKMP2 PES at 2.20 eV collision energy. For clarity of display, $P(J)$ for even j' are presented only.

transition state. The lower panel of Fig. 9 corresponds to collisions with zero impact parameter ($J=0$), and shows that for collinear configurations radial energy will promote recrossing instead of chemical reaction. In fact no reactivity is observed for initial bending angles higher than $\approx 155^\circ$. When all impact parameters are considered (upper panel), collinear reactivity is recovered, but still more recrossing than reactive trajectories are found for near collinear orientations. The reaction at $E_{\text{col}}=2.2$ eV has a broad cone of acceptance, and the maximum reactivity is found for bending angles in the 100° – 150° range.

An issue of current interest for the reactivity of this sys-

TABLE II. Total QCT cross sections (in \AA^2) for reactive (σ_{reactive}), nonreactive but recrossing (σ_{recross}) at various collision and total energies E_{col} and E_{tot} , respectively. N is the total number of trajectories run in each case.

E_{col} [eV]	Initial D ₂ state	E_{tot} [eV]	N	σ_{reactive} [\AA^2]	σ_{recross} [\AA^2]
2.20	($v=0, j=0$)	2.39	500 000	1.236(03)	0.577(02)
1.83	($v=1, j=0$)	2.39	50 000	1.875(14)	0.540(08)
2.67	($v=0, j=0$)	2.86	50 000	1.170(10)	0.802(09)

tem at high energies is the possible experimental detection of Geometric Phase effects in the dynamics. At present, the only experimental evidence supporting the appearance of GP effects for the hydrogen atom exchange reaction comes from the state specific rate constants measured by Zare and co-workers for $\text{D}+\text{H}_2(v=1)$ at a total energy of 1.82 eV.^{23,24} Other tentative assignments of experimental features³⁵ to GP effects²² were discarded after more refined experiments and calculations.^{3,36} In the just mentioned experiment by Zare and co-workers,^{23,24} notably colder rotational distributions were obtained. The discrepancies between these measurements and the QM and QCT results were much debated.^{37–39} The explicit inclusion of the GP in the QM calculations²⁰ made the discrepancies between the mentioned experiment and theory smaller.^{23,24} On the other hand, some uncertainties were also detected in the experimental data (see comments in Ref. 24). In a recent work, Adhikari and Billing⁴⁰ performed QCT calculations for the conditions of this ex-

periment using a treatment based on a vector potential in order to account approximately for GP effects in classical mechanics. Their results are also in better agreement with the measurements and with the GP QM data than with those from non-GP QM and QCT⁴¹ calculations. On the other hand, the highest resolution measurements available up to date, which correspond to collision energies of 0.52–0.54 eV, 1.27–1.30 eV, 2.20 eV, and 2.67 eV,^{1,2,4–6} could be well reproduced with dynamical calculations (both QM and/or QCT) that did not incorporate GP effects. An experimental reinvestigation of the $\text{D}+\text{H}_2(v=1, j=1) \rightarrow \text{HD}(v'=1, j')$ reaction under the conditions of Refs. 23,24 could be decisive for the assessment of GP effects in the reactivity of this system.

V. CONCLUSIONS

The fact that the extensive set of rovibrationally state-resolved differential cross sections measured in the present work for the $\text{H}+\text{D}_2(v=0, j=0) \rightarrow \text{HD}(v', j') + \text{D}$ reaction can be reproduced to a very high level of detail with the results of accurate QM scattering calculations on the BKMP2 potential surface seems to corroborate further that this surface is adequate for the quantitative description of the dynamics of the H_3 reactive system.

The global good agreement found between the measurements and the results of the QCT calculations shows that classical mechanics constitutes a good approximation for the description of the nuclear motion during reactive encounters at the high collision energy (2.2 eV) investigated.

For this collision energy, an efficient channeling of orbital angular momentum into rotational motion of the nascent molecules is observed, except for the highest vibrational states of HD. The correlation between sideways to forward scattering and high rotational excitation found in theoretical calculations is demonstrated experimentally. Noncollinear trajectories, leading to a broad angular distribution with a maximum in the sideways direction, are responsible for most of the reactivity. Collinear encounters lead predominantly to nonreactive recrossing, especially for low impact parameter collisions.

The excellent agreement found between experimental and QM calculations with no inclusion of the Geometrical Phase indicates that Geometric Phase effects will not be very important at this collision energy for the title reaction. A detailed experimental reinvestigation of the $\text{D}+\text{H}_2(v=1, j=1) \rightarrow \text{HD}(v'=1, j') + \text{H}$ reaction at a collision energy around 1 eV would be very clarifying, since it provides at present the experimental evidence for Geometric Phase ef-

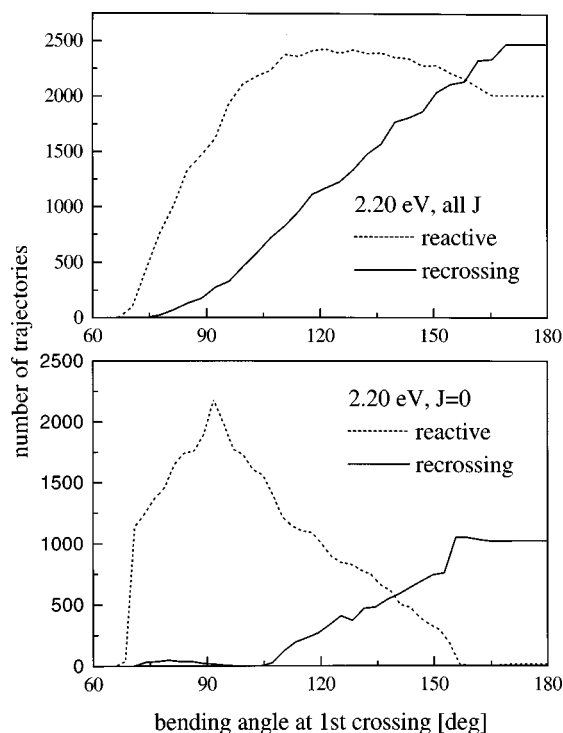


FIG. 9. Number of reactive and recrossing trajectories as a function of the bending angle at the first crossing (see text). Collinear configuration corresponds to 180°. Upper panel: trajectories covering the whole range of impact parameters leading to reaction ($0 < b < 1.3 \text{\AA}$). Lower panel: trajectories run with zero angular momentum (impact parameter).

fects, which have proven elusive under the conditions of all the higher resolution measurements of rovibrationally resolved differential cross sections.

ACKNOWLEDGMENTS

J.F.C. and B.M.H. acknowledge financial support through the program “Acciones para la Incorporación de Doctores y Tecnólogos” of the Ministry of Education and Culture of Spain. We also gratefully acknowledge the computer resources (Cray T-90) provided by the Leibniz Rechenzentrum in Munich (Germany). The German part of this work was funded by the German Science Foundation (Grant No. SCH 435/3) and the Deutscher Akademischer Austauschdienst (“Acciones Integradas”). The Spanish part was financed by the DGICYT (PB95-0918-C03) and by the “Acciones Integradas” Program of the Ministry of Education and Culture.

- ¹L. Schnieder, K. Seekamp-Rahn, J. Borkowski, E. Wrede, K. H. Welge, F. J. Aoiz, L. Bañares, M. J. D'Mello, V. J. Herrero, V. Sáez Rábanos, and R. E. Wyatt, *Science* **269**, 207 (1995).
- ²L. Schnieder, K. Seekamp-Rahn, E. Wrede, and K. H. Welge, *J. Chem. Phys.* **107**, 6175 (1997).
- ³E. Wrede and L. Schnieder, *J. Chem. Phys.* **107**, 786 (1997).
- ⁴E. Wrede, L. Schnieder, K. H. Welge, F. J. Aoiz, L. Bañares, and V. J. Herrero, *Chem. Phys. Lett.* **265**, 129 (1997).
- ⁵E. Wrede, L. Schnieder, K. H. Welge, F. J. Aoiz, L. Bañares, V. J. Herrero, B. Martínez-Haya, and V. Sáez Rábanos, *J. Chem. Phys.* **106**, 7862 (1997).
- ⁶L. Bañares, F. J. Aoiz, V. J. Herrero, M. J. D'Mello, B. Niederjohann, K. Seekamp-Rahn, E. Wrede, and L. Schnieder, *J. Chem. Phys.* **108**, 6160 (1998).
- ⁷L. Schnieder, W. Meier, K. H. Welge, M. N. R. Ashfold, and C. M. Western, *J. Chem. Phys.* **92**, 7027 (1990).
- ⁸B. Liu, *J. Chem. Phys.* **58**, 1925 (1973); P. Siegbahn and B. Liu, *ibid.* **68**, 2457 (1978).
- ⁹D. G. Truhlar and C. J. Horowitz, *J. Chem. Phys.* **68**, 2466 (1978); *ibid.* **71**, 1514(E) (1979).
- ¹⁰A. J. C. Varandas, F. B. Brown, C. A. Mead, D. G. Truhlar, and B. C. Garrett, *J. Chem. Phys.* **86**, 6258 (1987).
- ¹¹A. I. Boothroyd, W. J. Keogh, P. G. Martin, and M. R. Peterson, *J. Chem. Phys.* **95**, 4343 (1991).
- ¹²A. I. Boothroyd, W. J. Keogh, P. G. Martin, and M. R. Peterson, *J. Chem. Phys.* **104**, 7139 (1996).
- ¹³S. L. Mielke, G. C. Lynch, D. G. Truhlar, and D. W. Schwenke, *J. Phys. Chem.* **98**, 8000 (1994).
- ¹⁴J. Chang and N. Brown, *J. Phys. Chem.* **100**, 17740 (1996).
- ¹⁵F. J. Aoiz, L. Bañares, T. Díez-Rojo, V. J. Herrero, and V. Sáez Rábanos, *J. Phys. Chem.* **100**, 4071 (1996).
- ¹⁶F. J. Aoiz, L. Bañares, V. J. Herrero, V. Sáez Rábanos, and I. Tanarro, *J. Phys. Chem.* **101**, 6165 (1997).
- ¹⁷L. Bañares and M. J. D'Mello, *Chem. Phys. Lett.* **277**, 465 (1997).
- ¹⁸A. Kuppermann and Y.-S. M. Wu, *Chem. Phys. Lett.* **241**, 229 (1995).
- ¹⁹Y.-S. M. Wu, A. Kuppermann, and B. Lepetit, *Chem. Phys. Lett.* **186**, 319 (1991).
- ²⁰Y.-S. M. Wu and A. Kuppermann, *Chem. Phys. Lett.* **201**, 178 (1993).
- ²¹A. Kuppermann and Y.-S. M. Wu, *Chem. Phys. Lett.* **205**, 577 (1993); *ibid.* **213**, 636E (1993).
- ²²Y.-M. Wu and A. Kuppermann, *Chem. Phys. Lett.* **235**, 105 (1995).
- ²³D. A. V. Kliner and R. N. Zare, *J. Chem. Phys.* **92**, 2107 (1990).
- ²⁴D. A. V. Kliner, D. E. Adelman, and R. N. Zare, *J. Chem. Phys.* **95**, 1648 (1991).
- ²⁵D. E. Adelman, H. Xu, and R. N. Zare, *Chem. Phys. Lett.* **203**, 573 (1993).
- ²⁶H. Xu, N. E. Shafer-Ray, F. Merkt, D. J. Hughes, M. Springer, R. P. Tuckett, and R. N. Zare, *J. Chem. Phys.* **103**, 5157 (1995).
- ²⁷J. F. Castillo, D. E. Manolopoulos, K. Stark, and H.-J. Werner, *J. Chem. Phys.* **104**, 6531 (1996).
- ²⁸E. Wrede, Ph. D. Thesis, Universität Bielefeld, Verlag Hans Jacobs, Lage (1998).
- ²⁹F. J. Aoiz, V. J. Herrero, and V. Sáez Rábanos, *J. Chem. Phys.* **94**, 7991 (1991).
- ³⁰F. J. Aoiz, V. J. Herrero, and V. Sáez Rábanos, *J. Chem. Phys.* **97**, 7423 (1992).
- ³¹F. J. Aoiz, L. Bañares, M. J. D'Mello, V. J. Herrero, V. Sáez Rábanos, L. Schnieder, and R. E. Wyatt, *J. Chem. Phys.* **101**, 5781 (1994).
- ³²The complete set of experimental and theoretical v', j' state-resolved DCSs is available from the authors upon request.
- ³³F. J. Aoiz, L. Bañares, and V. J. Herrero, *J. Chem. Phys.* **105**, 6086 (1996).
- ³⁴F. J. Aoiz, L. Bañares, and V. J. Herrero, in *Advances in Classical Trajectory Methods, Vol. III: Comparison of Classical and Quantum Dynamics*, edited by W. L. Hase (JAI, Connecticut, 1998).
- ³⁵T. N. Kitsopoulos, M. A. Buntine, D. P. Baldwin, R. N. Zare, and D. W. Chandler, *Science* **260**, 1605 (1993).
- ³⁶A. Kuppermann and Y. M. Wu, private communication, quoted as Ref. 23 in Ref. 3.
- ³⁷N. C. Blais, M. Zhao, D. G. Truhlar, D. W. Schwenke, and D. J. Kouri, *Chem. Phys. Lett.* **166**, 368 (1990); *ibid.* **188**, 368E (1992).
- ³⁸S. L. Mielke, R. S. Friedman, D. G. Truhlar, and D. W. Schwenke, *Chem. Phys. Lett.* **188**, 359 (1992).
- ³⁹W. J. Keogh, A. I. Boothroyd, P. G. Martin, S. L. Mielke, D. G. Truhlar, and D. W. Schwenke, *Chem. Phys. Lett.* **195**, 144 (1992).
- ⁴⁰S. Adhikari and G. D. Billing, *J. Chem. Phys.* **107**, 6213 (1997); *Chem. Phys. Lett.* **284**, 31 (1998).
- ⁴¹F. J. Aoiz, H. K. Buchenau, V. J. Herrero, and V. Sáez Rábanos, *J. Chem. Phys.* **100**, 2789 (1994).